

OGAN: Disrupting Deepfakes with an Adversarial Attack that Survives Training

Eran Segalis
Independent Scholar
segaliseran@gmail.com

Eran Galili
Independent Scholar
Eran.Galili.Academic@gmail.com

Abstract—Recent advances in autoencoders and generative models have given rise to effective video forgery methods, used for generating so-called “deepfakes”. Mitigation research is mostly focused on post-factum deepfake detection and not on prevention. We complement these efforts by introducing a novel class of adversarial attacks—training-resistant attacks—which can disrupt face-swapping autoencoders whether or not its adversarial images have been included in the training set of said autoencoders. We propose the Oscillating GAN (OGAN) attack, a novel attack optimized to be training-resistant, which introduces spatial-temporal distortions to the output of face-swapping autoencoders. To implement OGAN, we construct a bilevel optimization problem, where we train a generator and a face-swapping model instance against each other. Specifically, we pair each input image with a target distortion, and feed them into a generator that produces an adversarial image. This image will exhibit the distortion when a face-swapping autoencoder is applied to it. We solve the optimization problem by training the generator and the face-swapping model simultaneously using an iterative process of alternating optimization. Next, we analyze the previously published Distorting Attack and show it is training-resistant, though it is outperformed by our suggested OGAN. Finally, we validate both attacks using a popular implementation of FaceSwap, and show that they transfer across different target models and target faces, including faces the adversarial attacks were not trained on. More broadly, these results demonstrate the existence of training-resistant adversarial attacks, potentially applicable to a wide range of domains.

1. Introduction

Recent improvements in deep learning have contributed to the rise of questionable applications that perform synthetic image rendering, known as deepfakes. They are used maliciously in various ways, from “face swapping” - replacing a person’s face in a video with another to misrepresent the target [25] to “face reenactment” [23] - which alters the expressions of a target person in a video by transferring the expressions of a source person to the target.

Efforts to combat such deepfake systems have mostly focused on detection [6, 12, 16, 19, 28, 29, 33], rather than prevention. While identifying content as fraudulent is important, when it comes to content that besmirches a



Figure 1: **OGAN visualization.** In the top row, a pristine image, followed by the OGAN-protected image, and a visualization for their difference. In the bottom row, a deepfake model applied to these two images, and the difference of its outputs. In the source data we see no observable difference, while in the deepfaked data we see a significant artifact - these artifacts create visible oscillations in videos.

person’s reputation - its mere existence might mean that the damage is already done.

Recently, a new approach to prevent deepfakes has surfaced - implementing adversarial attacks on the malicious deepfake models. An adversarial attack on a given model involves applying minute changes to a given input that are imperceptible by a human, but should the model be applied to the modified input, its output would be erroneous. Two examples of such successful attacks against deepfake systems have been shown in [20, 31].

Such adversarial attacks are effective in defeating deepfakes when the model is unlikely to be trained on data that includes the adversarial samples. Unfortunately, this assumption does not always hold. For example, in a fake news scenario such as [24], a deceiver might train a face-swapping model from scratch on videos of a political figure, in order to swap their face with another. Protecting the political figure’s videos by injecting adversarial samples would cause these samples to be included in the deepfake model’s training set, which could thwart the attack.

In this work, we propose a new family of attacks: *training-resistant adversarial attacks*. These attacks are similarly applied against a given model to produce adversarial samples, but they are a stronger form of adversarial attacks since they survive training. When the attacked model is applied to these samples, it will yield an erroneous output, whether or not these adversarial samples were included in its training data.

We demonstrate such a training-resistant attack against the face-swapping application of deepfake. We chose to focus on this application both because of the increasingly widespread usage of face-swapping in deepfakes, and because face-swapping is a good representative case of a deepfake model, and a successful attack on it could likely be generalized to more applications.

Our attack aims to inject minute perturbations to source video frames, so that when a face-swapping model is applied to them, the output includes visible spatial-temporal distortions that warps it, making the swap evident to a human eye (Figure 1). To achieve this goal and the property of training resistance, we formulate the objective as a general bilevel optimization problem, where we train a face-swapping model instance and an adversarial sample generator against each other; we choose this path over a more specific Minimax problem to avoid modifying the *FaceSwap* autoencoder’s loss function, while keeping the flexibility to modify the adversarial network’s loss function, and direct it toward generating samples that result in effective disruptions.

Our main contributions are:

- We introduce the concept of *training resistant adversarial attack*, motivated by real world deepfake applications where the training process of the model will likely include adversarial examples generated to defeat it.
- We study the Distorting Attack by Yeh *et al.* [31], and empirically show it satisfies the training resistance property.
- We propose the *Oscillating GAN (OGAN)* attack method, which improves on this previous work.
- We evaluate OGAN and the Distorting Attack on several implementations of face-swapping, the most popular deepfake system, and show OGAN outperforms it in scenarios where the attacked model’s training set includes the adversarial samples.

2. Related Work

Adversarial attacks had been extensively studied in the context of classification problems [1, 2, 4, 9, 14, 15, 17, 21, 26], but less research was published on their effect on generative models and autoencoders [8, 13, 22]. Tabacof *et al.* [8, 22] and Kos *et al.* [13] explore adversarial attacks against Variational Autoencoders (VAE), where Autoencoders and VAE-GAN models are used for image compression. Wang *et al.* [27] adapt adversarial attacks to image-to-image translation tasks under both paired and unpaired settings. Additionally for the paired setting they adapt a poisoning

attack on the target domain. Yeh *et al.* [31] and Ruiz *et al.* [20] are two concurrent works to ours, which explore adversarial attacks to disrupt deepfake models. Yeh *et al.* propose a Distorting attack in which the image translation model output becomes corrupt and a Nullifying attack in which the model becomes the identity mapping. Ruiz *et al.* [20] explore distorting attacks and extend them to conditional image translation networks. Additionally they adapt adversarial training [15] for conditional image translation GANs. Willetts *et al.* [30] explore defenses against adversarial attacks for VAE.

All of these attacks assume that the target models were trained using pristine data, a reasonable assumption for many applications. Unfortunately, for many other deepfake tasks this assumption doesn’t hold. For example, in a face-swapping scenario, a deceiver aims to swap the faces of A and B for some video v_A , which requires training a specific $A \rightarrow B$ model, and therefore collecting the corresponding training data. Since, in this scenario, v_A is available to the deceiver, the training data is likely to include images from v_A - which is the video we aim to protect, and therefore, will contain our adversarial images. Such cases may pose a challenge to attacks proposed by earlier works, which did not study the effect of the target model training on the adversarial images.

Consequently, an effective attack on this scenario should assume adversarial images might be included in the training data so the attack must be training-resistant, as defined in section 1. On the other hand, unlike in a poisoning attack (where one aims to poison the training data with bad inputs), our training-resistant attack should also assume that they might not be there, and succeed either way. This independence makes our attack more robust.

In this work, we first study the distorting attack by Yeh *et al.* [31], and show that it has the training-resistant property. In addition, we propose a new attack, OGAN, which has been optimized specifically for training resistance - and finally, we show that OGAN outperforms the distorting attack in cases where training resistance is required (defeating deepfakes). To the best of our knowledge, we are the first to introduce and study the notion of training-resistant adversarial attacks in any domain.

3. Method

3.1. DeepFake generation

While the term deepfake has become synonymous with its result of replacing a face in a video, it also refers to a specific face swapping method. The most notable implementation of this method is FaceSwap [25], as has been analyzed by [19] and many others. In this section, we will briefly describe this implementation of deepfake, an overview of which is shown in Figure 2.

This system receives as input an image sequence featuring source face A (a video, in this context, is viewed as an image sequence), and a sequence featuring target face B. First, an

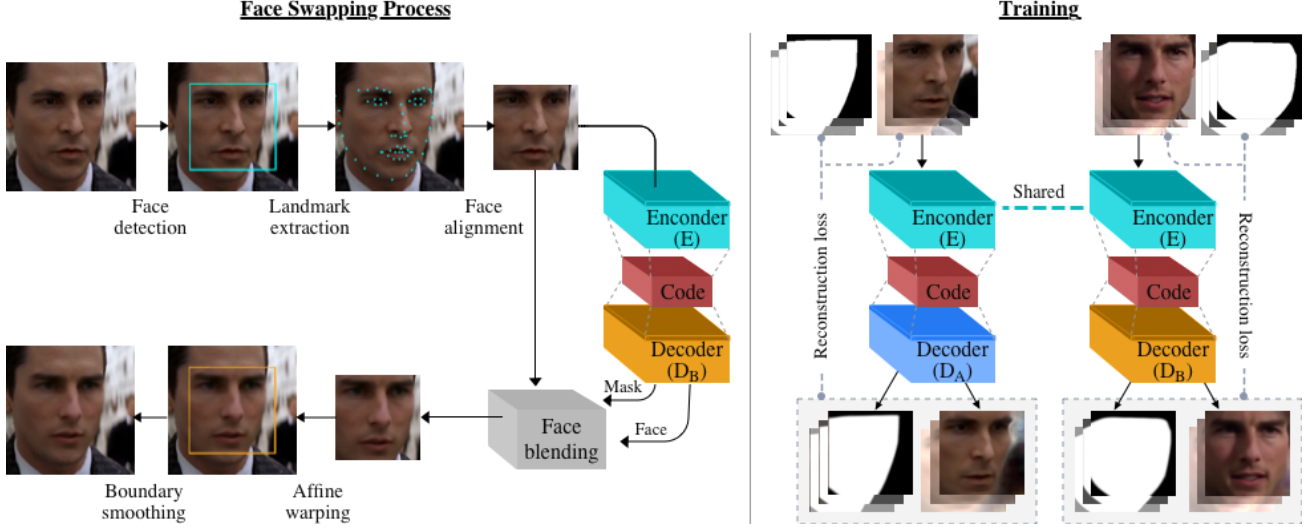


Figure 2: **Face swapping overview:** The application and training processes of the face swapping process. For further details, see section 3.1.

extraction phase extracts the faces from the images, aligns them, and creates masks that indicate where each face is located in each image. Next, two autoencoders with a shared encoder are trained to reconstruct images of the source and target faces. These autoencoders are trained on an augmentation of the input images, created via rotations, translations, magnifications and minute random color changes. Then, they are optimized using a reconstruction loss function, which consists of a mask loss function and a face loss function which is weighted by the input mask. The reconstruction loss function is thus defined as follows:

$$\mathcal{L}_{rec}(x^{face}, x^{mask}, y, m) = \mathcal{L}_{face}(x^{face}, y, m) \quad (1)$$

$$+ \mathcal{L}_{mask}(x^{mask}, m)$$

$$\mathcal{L}_{face}(x^{face}, y, m) = \|(x^{face} - y) \odot m\|_1 \quad (2)$$

$$\mathcal{L}_{mask}(x^{mask}, m) = \|x^{mask} - m\|_1 \quad (3)$$

where x^{face} and x^{mask} are the predicted face and mask, y is the input image, m is the input mask and \odot denotes a point-wise multiplication. We will refer to this loss function as the FaceSwap loss.

This yields an encoder and decoder pair for both face A and face B, where the decoders output both an image and face mask.

Finally, a swapped face is produced by applying the trained encoder and decoder of face B to the target images of face A. The output face is blended into the target image using the face mask.

DeepFake architectures. FaceSwap [25] offers several autoencoder architectures and configurations, but training a FaceSwap model is an expensive task that requires several days on high-end GPUs. Hence, a full evaluation of all the models is beyond the scope of this paper. Accordingly, we chose 3 architectures for our research:

- **realface:** This architecture uses skip connections for both its encoder and its decoders. It also uses an unbalanced framework where the autoencoder for the target face B has additional layers.
- **dfl-h128:** DeepFaceLab [11] is the one of the most popular deepfake implementations. This model includes a 128×128 pixels input model without skip connections, and closely reassembles the original model implemented in FaceSwap [25].
- **dfl-sae:** Another DeepFaceLab [11] architecture, this one uses skip connections only for the decoders.

These models provide us with diverse architecture types and represent the two most popular implementations of deepfake - [25, 11].

3.2. Optimization problem formulation

Our system’s objective is to add a tamper-evident feature to videos, disrupting attempts to manipulate them using deepfake. Thus, for a given video v including the face A , our system will output a modified video \bar{v} , where the differences between v and \bar{v} are imperceptible to a human observer. However, when the deepfake system is executed on \bar{v} with some target face B , the resulting $f_B(\bar{v})$ will include, instead of a seamless replacement of A with B , major human-visible artifacts identifying the deepfake tampering performed - thus defeating the attempted face swapping.

To achieve this goal, we use a class of disruptions to modify each frame in video v which are imperceptible in \bar{v} , but cause a change in the location, scaling and angle of face B in $f_B(\bar{v})$ - a change we represent using an affine transformation, N .

To formulate this, we define an adversarial generator $G(x, N)$ which receives as input a face image x and the

target affine transformation N . $G(x, N)$ outputs a modified face image satisfying:

$$G(x, N) = \arg \min_y \mathcal{L}_{adv}(y, x, N, m) \quad (4)$$

$$\text{s.t. } \|y - x\|_\infty \leq \varepsilon \quad (5)$$

Where ε is used to control the magnitude of the adversarial perturbation which is common in adversarial settings [9], and \mathcal{L}_{adv} is the adversarial loss function defined by:

$$\mathcal{L}_{adv}(x_{adv}, x, N, m) = \mathcal{L}_{face}(f_A^{face}(x_{adv}), N(x), m) \quad (6)$$

Where x and m are the original face image and mask, x_{adv} is the pertubated face image, f_A^{face} is the face output of the autoencoder f_A for face A and N is the target affine transformation.

For the adversarial loss, we use the autoencoder f_A of face A . We do this to keep the adversarial loss an internal process, i.e. defined by face A as much as possible, since an internal process will likely increase the odds for transferability of our adversarial attack to target faces other than B .

Now, let $\mathcal{D}_A, \mathcal{D}_B$ be the datasets used for training the FaceSwap autoencoders for faces A and B . Let $\mathcal{P}_A \subseteq \mathcal{D}_A$ be the subset of data we can control and would like to protect. For each $(x, m_x) \in \mathcal{P}_A$ we pick a distortion transformation N_x . We aim to find an adversarial generator such that:

$$G^* = \arg \min_G \sum_{(x, m_x) \in \mathcal{P}_A} \mathcal{L}_{adv}(G(x, N_x), x, N_x, m_x) \quad (7)$$

$$\text{s.t. } (f_A, f_B) \in \left\{ \arg \min_{f_A, f_B} \mathcal{L}_B(\mathcal{D}_B) + \mathcal{L}_A(\mathcal{D}'_A) \right\}$$

Where \mathcal{L}_A and \mathcal{L}_B are the FaceSwap losses for faces A and B as defined by:

$$\mathcal{L}_A(\mathcal{D}) = \sum_{(x, m_x) \in \mathcal{D}} \mathcal{L}_{rec}(f_A^{face}(x), f_A^{mask}(x), x, m_x) \quad (8)$$

$$\mathcal{L}_B(\mathcal{D}) = \sum_{(x, m_x) \in \mathcal{D}} \mathcal{L}_{rec}(f_B^{face}(x), f_B^{mask}(x), x, m_x) \quad (9)$$

Where $f_A^{face}, f_A^{mask}, f_B^{face}, f_B^{mask}$ are the face and mask outputs from the autoencoders f_A and f_B of faces A and B accordingly. \mathcal{D}'_A consists of the images from \mathcal{P}_A pertubated by G and the rest of the images of \mathcal{D}_A . More formally:

$$\mathcal{D}'_A = \{(G(x, N_x), m_x) \mid (x, m_x) \in \mathcal{P}_A\} \cup (\mathcal{D}_A \setminus \mathcal{P}_A) \quad (10)$$

Remark. An important factor in our problem formulation is the exclusion of the ℓ_∞ constraint. This is due to our design of G , in which we enforce the ℓ_∞ constraint of Equation 5 via the network architecture itself.

Algorithm 1: OGAN training algorithm

```

1 for  $iter = 1$  to  $T$  do
2   | Train autoencoders  $f_A$  and  $f_B$  on a single batch
3 end
4 for  $p$  in  $\mathcal{P}_A$  do
5   |  $N_p \leftarrow$  Sample random affine transformation
6 end
7 for  $epoch = 1$  to  $M$  do
8   | for  $i = 1$  to number of batches in  $\mathcal{P}_A$  do
9     |  $b_p, b_m, b_N \leftarrow$   $\mathcal{P}_A$ -batch: images, masks and
10    | transformations
11    | for  $i = 1$  to  $BatchSize$  do
12    |   |  $b'_{p,i} \leftarrow b_{N,i}(b_{p,i})$  // Transform face
13    | end
14    | for  $k = 1$  to  $BatchIters$  do
15    |   | // Train  $G$  on batch
16    |   |  $G \leftarrow opt_G(b_p, b_N, b'_p)$ 
17    | end
18    |  $b_p^{adv} \leftarrow G(b_p, b_N)$ 
19    |  $b_p^{aug}, b_m^{aug} \leftarrow Augment(b_p^{adv}, b_m)$ 
20    |  $f_A \leftarrow opt_{f_A}(b_p^{aug}, b_m^{aug})$ 
21    |  $c_p^{aug}, c_m^{aug} \leftarrow$  Augmented  $\mathcal{D}_B$ -batch
22    |  $f_B \leftarrow opt_{f_B}(c_p^{aug}, c_m^{aug})$ 
23    | end
24    | for  $i = 1$  to number of batches in  $(\mathcal{D}_A \setminus \mathcal{P}_A)$  do
25    |   |  $b_p^{aug}, b_m^{aug} \leftarrow$  Augmented  $\mathcal{D}_A$ -batch
26    |   |  $f_A \leftarrow opt_{f_A}(b_p^{aug}, b_m^{aug})$ 
27    |   |  $c_p^{aug}, c_m^{aug} \leftarrow$  Augmented  $\mathcal{D}_B$ -batch
28    |   |  $f_B \leftarrow opt_{f_B}(c_p^{aug}, c_m^{aug})$ 
29    | end
30  | end
31 end
32 return  $G, \{N_p\}$ 

```

3.3. Training procedure

Next, we proceed to the design of the training algorithm. We begin by training a FaceSwap model for T iterations, resulting in the autoencoders f_A and f_B for faces A and B respectively.

We continue by selecting a family of affine transformations $\{N_p\}$, for the target disruptions we plan on inducing. We first define the parameters Θ and Ψ , and then for each image p , we uniformly sample from $[-\Theta, \Theta]$ and $[-\Psi, \Psi] \times [-\Psi, \Psi]$ a rotation angle θ and shift (ψ_x, ψ_y) respectively, and define N_p to be the affine transformation operating on p by rotating it by θ , then shifting it by (ψ_x, ψ_y) .

For the next part of the training algorithm, we note that our bilevel optimization problem is closely related to the one used in poisoning attacks such as [18]. Therefore, we similarly solve the optimization problem by running an iterative process of alternating optimization of both G (via the adversarial loss \mathcal{L}_{adv}) and f_A, f_B (via the FaceSwap losses $\mathcal{L}_A, \mathcal{L}_B$), as a starting point for this process we use a

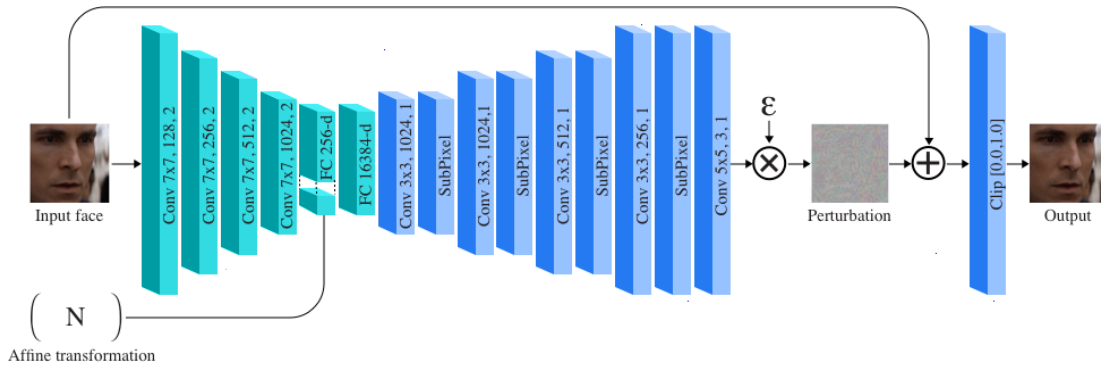


Figure 3: OGAN generator architecture.

random initialization for our generator G and for the FaceSwap autoencoders f_A, f_B we use autoencoders obtained from training a FaceSwap model for T iterations.

Finally, in order to stabilize the training process and to achieve stronger distortions of the output, we allow our generator extra training cycles for each batch we train on. The resulting algorithm is summarized in Algorithm 1.

Network architecture. For our adversarial generator, we choose to rely on the work in [2, 7] and use an autoencoder architecture. Specifically, we adapted the dfl-h128 autoencoder used in FaceSwap [25], which we’ve chosen since it is the model we train against in Algorithm 1. To address the ℓ_∞ constraint, we use \tanh non-linearity in our last convolutional layer and multiply the result by ε . A detailed description of the generator network’s architecture is shown in figure 3.

3.4. Distorting attack

Yeh *et al.* [31] and Ruiz *et al.* [20] have proposed an adversarial attack on image translation models (a class that includes FaceSwap). This Distorting Attack defines its adversarial loss as a function that aims to move a target model’s output for an adversarial example as far as possible from its output for the original example. Next, the attack utilizes Projected Gradient Descent (PGD) [15] to generate the adversarial samples (the protected images) from the original samples (the input images). More formally, let x be an input image, let H be an image translation model, let ε be a perturbation bounding parameter and α a learning rate parameter. PGD consists of a random initialization and an update rule:

$$\begin{aligned} x_0^{adv} &= x + \text{noise} \\ x_{t+1}^{adv} &= \text{clip}_{x,\varepsilon}(x_t^{adv} - \alpha \cdot \text{sign}(\nabla_{x^{adv}} \mathcal{L}(x_t^{adv}, x))) \end{aligned} \quad (11)$$

Where x_t^{adv} is the adversarial example at the t_{th} iteration, noise is a random vector of the same dimensions as x and whose elements are in $[-\varepsilon, \varepsilon]$, and $\text{clip}_{x,\varepsilon}(z)$ denotes element-wise clipping z , with $z_{i,j}$ clipped to the range $[x_{i,j} - \varepsilon, x_{i,j} + \varepsilon]$ and then clipped to valid image range and \mathcal{L} the adversarial loss used for the attack.

In the Distorting attack the adversarial loss \mathcal{L} equals the distortion loss \mathcal{L}_{dist} defined by:

$$\mathcal{L}_{dist}(x^{adv}, x) = -\|H(x^{adv}) - H(x)\|_2 \quad (12)$$

For our attack setting, $H(x)$ is the deepfaked image produced from x using the f_B autoencoder, specifically:

$$H(x) = f_B^{face}(x) \odot f_B^{mask}(x) + x \odot (1 - f_B^{mask}(x)) \quad (13)$$

Where \odot denotes a point-wise multiplication and f_B^{face}, f_B^{mask} are the face and mask outputs from the autoencoder f_B of face B .

4. Experiments

We evaluate our attack against the face-swapping models described in section 3.1, with some slight adjustments so the models would have the same input size and they could be trained with the same batch size while fitting in our GPU’s memory. First, we match the input size of the realface model to 128×128 . Next, we slightly decrease the sizes of realface (by setting dense_nodes to 1408) and dfl-h128 (by setting low_memory=True). This decrease in size should not affect the efficacy of our technique on the original models.

4.1. Datasets

We collected several videos from YouTube for 3 people A, B, C . For each person, we first extracted their face images from the videos using S³FD [32] and aligned them using FAN [3]. Then, we removed blurry images and the face images of other people appearing in the videos. This resulted in a set of about 5000 face images for each person; these are the datasets we will train FaceSwap models on, $\mathcal{D}_A, \mathcal{D}_B$ and \mathcal{D}_C . For the dataset of data we control, \mathcal{P}_A , we arbitrarily choose person A and focus on the subset of 444 of face A ’s images extracted from one of their videos, v_A . The remainder of face A ’s images, $\mathcal{D}_A \setminus \mathcal{P}_A$, emulates data a faceswapping deceiver might have access to, but which we do not control.

4.2. Generation of adversarial images

To generate the adversarial images from both OGAN and the Distorting Attack, we begin by training a FaceSwap model with the dfl-h128 architecture using the datasets \mathcal{D}_A and \mathcal{D}_B for $T = 200000$ iterations. The model is optimized with the Adam optimizer, configured with the following hyperparameters: $\beta_1 = 0.5$, $\beta_2 = 0.999$, a learning rate of 5×10^{-5} and a batch size of 64.

Next, for the Distorting Attack, we use the autoencoder f_B from this trained model to generate the adversarial images for the original face images in \mathcal{P}_A over 1000 iterations, with the hyperparameters: $\varepsilon = \frac{2}{255}$, $\alpha = 0.001$. This results in the adversarial image set we mark as O_A^{Dist} .

Finally, for OGAN, we train our generator against the trained FaceSwap model using Algorithm 1, with the FaceSwap model we’ve already trained, and the following hyperparameters: $\varepsilon = \frac{2}{255}$, $\Theta = 10$, $\Psi = 12.8$, $BatchSize = 64$, $BatchIters = 8$. The OGAN networks are also trained using the Adam optimizer with the following hyperparameters: $\beta_1 = 0.9$, $\beta_2 = 0.9999$, a learning rate of 5×10^{-5} and a batch size of 64. The generator has been trained for $M = 1024$ epochs using \mathcal{D}_A , \mathcal{P}_A and \mathcal{D}_B . As explained in Algorithm 1 above, this results in the trained adversarial generator, as well as the output affine transformations. We use these generator and transformations to calculate the adversarial images of the face images in \mathcal{P}_A , resulting in the adversarial image set O_A^{OGAN} .

Finally, we will patch the faces from both O_A^{OGAN} and O_A^{Dist} back onto their original video v_A . We do this so we are later able to simulate an end-to-end application of deepfake techniques on the videos. After patching the face images from each of O_A^{OGAN} and O_A^{Dist} onto v_A , we now have the adversarial videos (which are the protected videos) \bar{v}_A^{OGAN} and \bar{v}_A^{Dist} respectively.

4.3. Metrics

Spatial-temporal score. To quantitatively measure video distortion, and to evaluate OGAN and the Distorting Attacks, we use the temporal consistency metric E_{tmp} [10, 5]. This metric quantifies the overall differences between consecutive frames in a video by averaging the pixel-wise Euclidean difference in color between frames, as defined by:

$$E_{tmp}(y) = \gamma \sqrt{\frac{1}{d(n-1)} \sum_{i=1}^{n-1} \|y_{i+1} - y_i\|_2^2} \quad (14)$$

where y is a sequence of video frames, y_i is the i -th frame, n is number of frames in the video, d is the number of pixels in each frame and γ is a scaling constant, set to 10^3 [5].

Next, we note that consecutive video frames in a non-static video (meaning, a video which is not a sequence of identical images) would exhibit a natural spatial-temporal difference. Thus, in addition to E_{tmp} we compute S_{tmp} , which is the normalized E_{tmp} metric, to obtain a score

that’s independent of the specific video. S_{tmp} is computed by:

$$S_{tmp}(\bar{v}_{A \rightarrow K}, v_{A \rightarrow K}) = \frac{E_{tmp}(\bar{v}_{A \rightarrow K})}{E_{tmp}(v_{A \rightarrow K})} - 1 \quad (15)$$

Where K is a target face (either face B or face C), $v_{A \rightarrow K}$ is a deepfaked video of v_A (i.e. where we swapped face A to face K) and $\bar{v}_{A \rightarrow K}$ is deepfaked video of \bar{v}_A (where \bar{v}_A is the adversarial video obtained from v_A).

Since the ratio $\frac{E_{tmp}(\bar{v}_{A \rightarrow K})}{E_{tmp}(v_{A \rightarrow K})}$ is 1 if the adversarial attack did not impact the deepfake model’s output at all, we adjust S_{tmp} ’s range by subtracting 1 from the result.

4.4. Attacks evaluation

As before (section 4.1), we extract face images from \bar{v}_A^{OGAN} and \bar{v}_A^{Dist} using S³FD and FAN. We then combine each of these face image sets with the face images from $\mathcal{D}_A \setminus \mathcal{P}_A$ - resulting in the new datasets \mathcal{D}_A^{OGAN} and \mathcal{D}_A^{Dist} respectively.

Training resistance. We first evaluate the attacks against face swapping models trained using the datasets \mathcal{D}_A^{OGAN} and \mathcal{D}_A^{Dist} , which include our adversarial images. To do this, we train a dfl-h128 model for the task of face swapping $A \rightarrow B$ for each of these datasets. These models (and other face swapping models mentioned later in this section) were trained for 200000 iterations using the Adam optimizer with the following hyperparameters: $\beta_1 = 0.5$, $\beta_2 = 0.999$, a learning rate of 5×10^{-5} and a batch size of 64. The training was executed using the FaceSwap code [25] using its default hyperparameters, and the same number of training iterations as were used to generate the FaceForensics dataset [19], which is used for the detection of face swapped videos.

Figure 4 shows that injecting the OGAN adversarial perturbations to the pristine video creates a difference between consecutive frames that’s similar to white noise added to the natural difference between the matching pristine frames - this is why the perturbations are not observable in the adversarial source video. However, the difference between consecutive frames of this video after a deepfake model is applied to it resembles a face - this is because the attack caused the face’s location to shift. This shift is noticeable in the disrupted video, as can be seen in the video in the supplementary material. Perturbations injected by the Distorting Attack create a similar effect¹.

Next, we analyze the attacks performance, on the dfl-h128 FaceSwap models we trained, using S_{tmp} - see Table 1. These results show that even though the face swapping models are familiar with the adversarial images (i.e., their training data includes the adversarial images), both attacks successfully created major artifacts in the resulting video. However, OGAN’s impact on S_{tmp} is significantly greater.

1. See the first demo video in https://youtu.be/_XEcCtC7EEw



Figure 4: **Perturbation visualization.** Samples from a dfl-h128 face swapping model trained for 500000 iterations on \mathcal{D}_A^{OGAN} . First row from left to right: Pristine consecutive face images from our video, visualization of their difference, their face swapping outputs and a visualization of their difference. Second row from left to right: adversarial perturbations of the same consecutive images, visualization of their difference, their face swapping outputs and a visualization of their difference. This shows that the difference created by adding the adversarial perturbations to the pristine video resembles white noise and is thus not noticeable, but applying face swapping results in major, noticeable artifacts.

Method	S_{tmp}	E_{tmp}
Distorting '2020 [31]	0.019	46.265
OGAN (Ours)	0.061	48.212

Table 1: **Training resistance.** Spatial-temporal scores for attacked dfl-h128 face-swapping models, trained for 200000 iterations on the \mathcal{D}_A^{OGAN} and \mathcal{D}_A^{Dist} datasets (which includes our adversarial images). The S_{tmp} scores shows both attacks are training resistant, with OGAN performing significantly better.

Attack transferability. Next, we analyze the transferrability of the attacks across faceswapping architectures. For this, we train both the dfl-sae and realface models for $A \rightarrow B$ for each attack. Additionally, we train another dfl-h128 model for $A \rightarrow C$ so we can evaluate the transferability of the attacks across different target faces.

The results of applying OGAN and the Distorting Attack to these additional models are shown in Table 2. These results show that both attacks are applicable for different faceswap mode architectures, and for faces that the attacks were not trained on (i.e. for models swapping $A \rightarrow Z$ for some face Z). However, OGAN outperforms the Distorting Attack on both dfl-h128 and dfl-sae. For realface, both attacks achieve relatively similar S_{tmp} scores, with a slight advantage for the Distorting Attack.

Exclusion of adversarial images. Next, we validate that the attacks succeed even when their adversarial images are excluded from the face swapping model’s training set. While in this case, it is easier for an adversarial attack to succeed, success here will confirm that the attacks are training-resistant attacks, rather than poisoning attacks which requires injecting samples into the training process. We train dfl-h128, dfl-sae and realface on $\mathcal{D}_A \setminus \mathcal{P}_A$ and \mathcal{D}_B for the task of $A \rightarrow B$, and another dfl-h128 model for the task of $A \rightarrow C$. Training

Method	Attacked model	Swapping direction	Temporal scores: S_{tmp}	E_{tmp}
Distorting '2020 [31]	dfl-h128	$A \rightarrow C$	0.006	44.262
	dfl-sae	$A \rightarrow B$	0.059	48.160
	realface	$A \rightarrow B$	0.159	52.701
OGAN (Ours)	dfl-h128	$A \rightarrow C$	0.018	44.731
	dfl-sae	$A \rightarrow B$	0.075	48.892
	realface	$A \rightarrow B$	0.149	51.977

Table 2: **Transferability.** Spatial-temporal scores for attacks on face-swapping models of various architectures and target faces, trained for 200000 iterations on the \mathcal{D}_A^{OGAN} and \mathcal{D}_A^{Dist} datasets (which include our adversarial images). These results show OGAN achieves comparable or better results to the Distorting Attack on additional face swapping architectures, and on target faces the adversarial attack wasn’t trained on.

is performed in the same way as before, and S_{tmp} and E_{tmp} are calculated for each attack as applied to each model. As shown in Table 3, the Distorting Attack performs better than OGAN in this case. This is expected, since OGAN has been designed to focus on cases where the adversarial images are included. However, as reflected by the S_{tmp} scores, both attacks strongly outperform their results in the training resistant setting, as seen in Tables 1 and 2 and also in the greater magnitude of distortions in the second demo video².

Therefore we consider both attacks successful in this case.

Effect of extra training. Finally, we investigate the effect of training the face swapping models for additional iterations on \mathcal{D}_A^{OGAN} and \mathcal{D}_A^{Dist} . We train our dfl-h128 models on the task of $A \rightarrow B$ for an additional 300000 iterations, and

2. See the second demo video in <https://youtu.be/4dkwqWVZK0M>

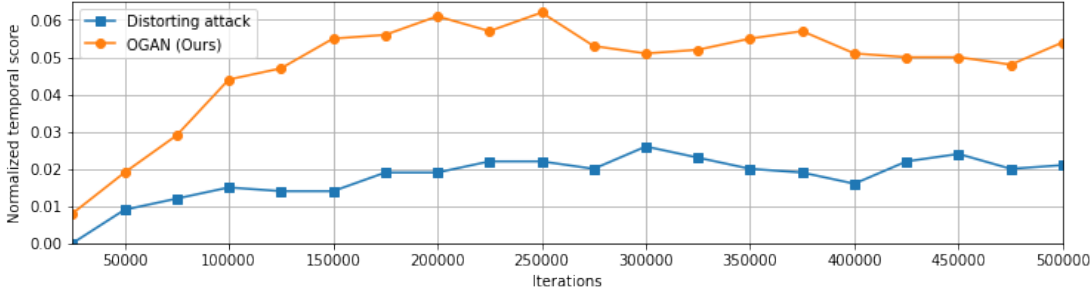


Figure 5: **Effect of extra training.** S_{tmp} scores for attacks on dfl-h128 face swapping models trained for 500000 iterations on the \mathcal{D}_A^{OGAN} and \mathcal{D}_A^{Dist} datasets, which contain the adversarial examples. This data shows that the S_{tmp} scores stabilize at around 300000 iterations, and the attacks remain successful even on a model trained for a larger number of iterations on data that includes the adversarial examples.

Method	Attacked model	Swapping direction	Temporal scores:	
			S_{tmp}	E_{tmp}
Distorting '2020 [31]	dfl-h128	$A \rightarrow B$	0.270	57.289
	dfl-h128	$A \rightarrow C$	0.078	44.993
	dfl-sae	$A \rightarrow B$	0.232	55.495
	realface	$A \rightarrow B$	0.359	61.706
OGAN (Ours)	dfl-h128	$A \rightarrow B$	0.184	53.562
	dfl-h128	$A \rightarrow C$	0.058	44.226
	dfl-sae	$A \rightarrow B$	0.169	52.765
	realface	$A \rightarrow B$	0.280	58.310

Table 3: **Exclusion of adversarial images.** Spatial-temporal scores for attacks on face-swapping models that were trained for 200000 iterations on $\mathcal{D}_A \setminus \mathcal{P}_A$, which does not contain any adversarial images. These results show that while OGAN was designed for the training resistant case and underperforms here, it still succeeds in achieving a large S_{tmp} score - despite the attack having no control on any part of the target model’s training set.

calculate S_{tmp} every 25000 iterations. As shown in Figure 5, the S_{tmp} score begins to stabilize after 300000 iterations of training, and even after 500000 iterations, $S_{tmp} > 0$, with a value of 0.021 for the Distorting attack and a better value of 0.054 for OGAN. These distortions are still highly noticeable, as can be observed in Figure 4. This result confirms that even a resourceful deceiver, capable of training for many iterations, will fail in manipulating \bar{v}_A^{OGAN} and \bar{v}_A^{Dist} due to the attacks.

5. Conclusions

In this work we introduced training-resistant adversarial attacks. These attacks generate adversarial samples against a given model such that when the model is applied to these samples, its intended effect is disrupted - even if the same adversarial samples were part of the model’s training data. This is a key difference between such attacks and poisoning attacks, since poisoning attacks require that the adversarial samples be part of the training data.

Additionally, we developed OGAN - an attack designed for training resistance, against face swapping autoencoders. We empirically showed that the Distorting Attack by Yeh *et al.* [31] also fulfills the training resistance property, and applied both this attack and OGAN end-to-end against commonly used FaceSwap implementations.

Our results show that both attacks transfer across different face swapping models and target faces, including target faces the adversarial attacks were not trained on. Our results also show that OGAN outperforms the Distorting Attack in the training resistant case - when the target model’s training data includes the adversarial samples, and that OGAN is also successful in the regular case - when the training data does not include the adversarial samples.

These results demonstrate the existence and feasibility of training-resistant adversarial attacks, potentially applicable to a wide range of domains.

Acknowledgements

The authors would like to thank Jonathan Heimann, Roy Iarchy and Orgad Keller for many fruitful discussions and comments.

References

- [1] Naveed Akhtar and Ajmal S. Mian. Threat of adversarial attacks on deep learning in computer vision: A survey. *IEEE Access*, 6:14410–14430, 2018.
- [2] Shumeet Baluja and Ian Fischer. Adversarial transformation networks: Learning to generate adversarial examples. *CoRR*, abs/1703.09387, 2017.
- [3] Adrian Bulat and Georgios Tzimiropoulos. How far are we from solving the 2d & 3d face alignment problem? (and a dataset of 230, 000 3d facial landmarks). In *ICCV*, pages 1021–1030. IEEE Computer Society, 2017.
- [4] Nicholas Carlini and David A. Wagner. Towards evaluating the robustness of neural networks. In *IEEE Symposium on Security and Privacy*, pages 39–57. IEEE Computer Society, 2017.

- [5] Chia-Chi Cheng, Hung-Yu Chen, and Wei-Chen Chiu. Time flies: Animating a still image with time-lapse video as reference. In *CVPR*, pages 5640–5649. IEEE, 2020.
- [6] Davide Cozzolino, Justus Thies, Andreas Rössler, Christian Riess, Matthias Nießner, and Luisa Verdoliva. Forensictransfer: Weakly-supervised domain adaptation for forgery detection. *CoRR*, abs/1812.02510, 2018.
- [7] Ji Feng, Qi-Zhi Cai, and Zhi-Hua Zhou. Learning to confuse: Generating training time adversarial data with auto-encoder. In *NeurIPS*, pages 11971–11981, 2019.
- [8] George Gondim-Ribeiro, Pedro Tabacof, and Eduardo Valle. Adversarial attacks on variational autoencoders. *CoRR*, abs/1806.04646, 2018.
- [9] Ian J. Goodfellow, Jonathon Shlens, and Christian Szegedy. Explaining and harnessing adversarial examples. In *ICLR (Poster)*, 2015.
- [10] Haozhi Huang, Hao Wang, Wenhan Luo, Lin Ma, Wenhao Jiang, Xiaolong Zhu, Zhifeng Li, and Wei Liu. Real-time neural style transfer for videos. In *CVPR*, pages 7044–7052. IEEE Computer Society, 2017.
- [11] iperov. Deepfacelab github., 2020. URL <https://github.com/iperov/DeepFaceLab>.
- [12] Ali Khodabakhsh, Ramachandra Raghavendra, Kiran B. Raja, Pankaj Shivdayal Wasnik, and Christoph Busch. Fake face detection methods: Can they be generalized? In *BIOSIG*, volume P-282 of *LNI*, pages 1–6. GI / IEEE, 2018.
- [13] Jernej Kos, Ian Fischer, and Dawn Song. Adversarial examples for generative models. In *IEEE Symposium on Security and Privacy Workshops*, pages 36–42. IEEE Computer Society, 2018.
- [14] Alexey Kurakin, Ian J. Goodfellow, and Samy Bengio. Adversarial examples in the physical world. In *ICLR (Workshop)*. OpenReview.net, 2017.
- [15] Aleksander Madry, Aleksandar Makelov, Ludwig Schmidt, Dimitris Tsipras, and Adrian Vladu. Towards deep learning models resistant to adversarial attacks. In *ICLR (Poster)*. OpenReview.net, 2018.
- [16] Francesco Marra, Diego Gragnaniello, Davide Cozzolino, and Luisa Verdoliva. Detection of gan-generated fake images over social networks. In *MIPR*, pages 384–389. IEEE, 2018.
- [17] Seyed-Mohsen Moosavi-Dezfooli, Alhussein Fawzi, Omar Fawzi, and Pascal Frossard. Universal adversarial perturbations. In *CVPR*, pages 86–94. IEEE Computer Society, 2017.
- [18] Luis Muñoz-González, Battista Biggio, Ambra Demontis, Andrea Paudice, Vasin Wongrassamee, Emil C. Lupu, and Fabio Roli. Towards poisoning of deep learning algorithms with back-gradient optimization. In *AISeC@CCS*, pages 27–38. ACM, 2017.
- [19] Andreas Rössler, Davide Cozzolino, Luisa Verdoliva, Christian Riess, Justus Thies, and Matthias Nießner. Faceforensics++: Learning to detect manipulated facial images. In *ICCV*, pages 1–11. IEEE, 2019.
- [20] Nataniel Ruiz, Sarah Adel Bargal, and Stan Sclaroff. Disrupting deepfakes: Adversarial attacks against conditional image translation networks and facial manipulation systems. *CoRR*, abs/2003.01279, 2020.
- [21] Christian Szegedy, Wojciech Zaremba, Ilya Sutskever, Joan Bruna, Dumitru Erhan, Ian J. Goodfellow, and Rob Fergus. Intriguing properties of neural networks. In *ICLR (Poster)*, 2014.
- [22] Pedro Tabacof, Julia Tavares, and Eduardo Valle. Adversarial images for variational autoencoders. *CoRR*, abs/1612.00155, 2016.
- [23] Justus Thies, Michael Zollhöfer, Marc Stamminger, Christian Theobalt, and Matthias Nießner. Face2face: Real-time face capture and reenactment of RGB videos. In *CVPR*, pages 2387–2395. IEEE Computer Society, 2016.
- [24] Rob Toews. Deepfakes are going to wreak havoc on society. we are not prepared., 2020. URL <https://www.forbes.com/sites/robtoews/2020/05/25/deepfakes-are-going-to-wreak-havoc-on-society-we-are-not-prepared/#2248f32b7494>.
- [25] Torzdf. Deepfakes github., 2020. URL <https://github.com/deepfakes/faceswap>.
- [26] Florian Tramèr, Alexey Kurakin, Nicolas Papernot, Ian J. Goodfellow, Dan Boneh, and Patrick D. McDaniel. Ensemble adversarial training: Attacks and defenses. In *ICLR (Poster)*. OpenReview.net, 2018.
- [27] Lin Wang, Wonjune Cho, and Kuk-Jin Yoon. Deceiving image-to-image translation networks for autonomous driving with adversarial perturbations. *IEEE Robotics Autom. Lett.*, 5(2):1421–1428, 2020.
- [28] Run Wang, Felix Juefei-Xu, Lei Ma, Xiaofei Xie, Yihao Huang, Jian Wang, and Yang Liu. Fakespotter: A simple yet robust baseline for spotting ai-synthesized fake faces. In *IJCAI*, pages 3444–3451. ijcai.org, 2020.
- [29] Sheng-Yu Wang, Oliver Wang, Richard Zhang, Andrew Owens, and Alexei A. Efros. Cnn-generated images are surprisingly easy to spot... for now. In *CVPR*, pages 8692–8701. IEEE, 2020.
- [30] Matthew Willetts, Alexander Camuto, Tom Rainforth, Stephen Roberts, and Chris Holmes. Improving vaes’ robustness to adversarial attack. *arXiv preprint arXiv:1906.00230*, 2019.
- [31] Chin-Yuan Yeh, Hsi-Wen Chen, Shang-Lun Tsai, and Shang-De Wang. Disrupting image-translation-based deepfake algorithms with adversarial attacks. In *WACV Workshops*, pages 53–62. IEEE, 2020.

- [32] Shifeng Zhang, Xiangyu Zhu, Zhen Lei, Hailin Shi, Xiaobo Wang, and Stan Z. Li. S³fd: Single shot scale-invariant face detector. *CoRR*, abs/1708.05237, 2017.
- [33] Peng Zhou, Xintong Han, Vlad I. Morariu, and Larry S. Davis. Two-stream neural networks for tampered face detection. In *CVPR Workshops*, pages 1831–1839. IEEE Computer Society, 2017.